Available online at www.sciencedirect.com
ScienceDirect
Journal of Power Sources 176 (2008) 222–228
JOURNAL OF POWER SOURCES
www.elsevier.com/locate/jpowsour

Simulation studies of the membrane exchange assembly of an all-liquid, proton exchange membrane fuel cell

Ethan D. Byrd [a,*], George H. Miley [b]

[a] Department of Electrical and Computer Engineering, University of Illinois at Urbana-Champaign, Everitt Laboratory, MC-702, 1406 W. Green St., Urbana, IL 61801-2918, USA
[b] Department of Nuclear, Plasma, and Radiological Engineering, University of Illinois at Urbana-Champaign, 100C NEL, 103 S. Goodwin Ave., Urbana, IL 61801, USA

Received 10 September 2007; received in revised form 18 October 2007; accepted 19 October 2007
Available online 1 November 2007

Abstract

A model has been designed and constructed for the all-liquid, sodium borohydride/hydrogen peroxide fuel cell under development at the University of Illinois at Urbana-Champaign. The electrochemical behavior, momentum balance, and mass balance effects within the fuel cell are modeled using the Butler–Volmer equations, Darcy's law, and Fick's law, respectively, within a finite element modeling platform. The simulations performed with the model indicate that an optimal physical design of the fuel cell's flow channel land area or current collector exists when considering the pressure differential between channels, and the diffusion layer permeability and conductivity. If properties of the diffusion layer are known, the model is an effective method of improving the fuel cell design in order to achieve higher power density.

Keywords: Fuel cell; Hydrogen peroxide; Sodium borohydride; Membrane exchange assembly

1. Introduction

A novel sodium borohydride/hydrogen peroxide ($NaBH_4/H_2O_2$) fuel cell is under development at the University of Illinois at Urbana-Champaign. The cell has distinct advantages for space applications due to the all-liquid nature and high energy density of the reactants. The $NaBH_4/H_2O_2$ fuel cell group at the University of Illinois has been working to steadily improve the design and capabilities of the cell [1–3]. Due to the novel nature of the fuel cell, there is a lack of modeling research into its characteristics, motivating this study.

The development of a model for the $NaBH_4/H_2O_2$ fuel cell is intended with the goal of understanding some of the characteristics that are important in the design. Specifically, the geometries of the fuel flow channels and the characteristics of the diffusion layer are considered. It is hoped that the cell performance and power output can be improved for later optimization by varying the geometries and physical characteristics of the cell and the diffusion layer. In this study, flow rates (indicative of pressure differentials), permeability, conductivity, and basic flow channel geometry are varied [4].

For reference throughout the paper, the balanced reaction equations for the $NaBH_4/H_2O_2$ fuel cell are shown in Eqs. (1) and (2).

$$NaBH_4 + 4H_2O \rightarrow NaBO_2\,2H_2O + 8H^+ + 8e^- \quad (1)$$

$$H_2O_2 + 2H^+ + 2e^- \rightarrow 2H_2O \quad (2)$$

2. Description of model

The model developed here employ the equations and geometries similar to those used in prior models [4–6]. As in those models, the system is set up with a series of differential equations to account for the various interactions occurring in the MEA; however, specific equations are adapted for use with the physics packages in the finite element modeling software [6]. The MEA consists of a diffusion layer, Nafion membrane, and another diffusion layer. Appropriate catalysts are deposited on the diffusion layers. First, the physical layout of the model used

* Corresponding author. Present address: 582 Williamsburg Ct. #B-2, Wheeling, IL 60090, USA. Tel.: +1 847 528 2747; fax: +1 217 333 2906.
E-mail addresses: ethan.byrd@gmail.com (E.D. Byrd), ghmiley@uiuc.edu (G.H. Miley).

0378-7753/$ – see front matter © 2007 Elsevier B.V. All rights reserved.
doi:10.1016/j.jpowsour.2007.10.077

Nomenclature

Electrical and Butler–Volmer terms

σ	conductivity
Φ	electric potential
i	current
i_0	exchange current density
n	moles of e^-
β	charge transfer coefficient
F	Faraday's constant
η	overpotential
R	universal gas constant
T	temperature
w^*	species concentration
w_0^*	species input concentration
α	reaction constant
f	temperature constant
$*_a$	anode subscript
$*_c$	cathode subscript
$*_{d1}$	anodic diffusion layer subscript
$*_{d2}$	cathodic diffusion layer subscript
$*_m$	membrane layer subscript
*eq	equilibrium superscript

Mass transport terms

D_i	species diffusion coefficient
R	reaction rate
u	fluid velocity
N_0	inward flux
n	normal vector
N	species input concentration
I	species concentration

Momentum balance terms

v'	mean fluid velocity
$k(\kappa)$	permeability
μ	viscosity
Δp (p_{diff})	pressure differential

is described, followed by a description of the equations modeling the physical phenomenon occurring in each component of the MEA.

An efficient method for modeling a large system is to look for repetitive structures and then model one of the smaller structures. This allows for the creation of simpler models, but care must be taken to ensure the boundaries of the structures are adequately considered. A drawback of modeling in this way is that the edge-effects of the larger system are not modeled. For PEM fuel cells with serpentine flow channels, the edge-effects are not as critical as the reaction rates in the repetitive array of flow channels, which contribute the most to the output power of the cell. The repetitive cross section chosen is from the midpoint of one flow channel to the midpoint of the next and extends across the two diffusion layers and the membrane. The flow in the flow channels are considered to be at constant concentration. This is a simplification, but reasonably accurate since, due to high flow rates and concentrated reactant, there is little concentration change between adjacent flow channels. For visualization purposes, Fig. 1 shows the cross section of the fuel cell that the model considers; each physical area is labeled. In the expanded repetitive section, the black outline indicates the portion that is modeled; thus, the flow channels are considered boundary conditions in the model. Portions of the graphite plate are part of the model to incorporate current flow through this region. Finally, the two diffusion layers and Nafion membrane are incorporated.

The model is a 2D approximation of the fuel cell, and is created and simulated using COMSOL Multiphysics. Once the model is physically created, it is described using built-in or user-defined differential equations. To describe the model, each region has coefficients for every differential equation (the coefficients may be zero if that particular equation does not interact in that region); also, the boundary conditions are described for each region where a differential equation is applied. The software has built-in applications that allow the regions to be easily described. For example, a simple DC current equation allows for constant voltage or current boundary conditions, while also indicating the resistance in the region. More complicated dependencies can be set up by having the resistance be a function of some other element, such as temperature, although temperature was not considered in this model.

The software then generates a 2D triangular mesh containing thousands of elements. Using finite element analysis, the software converges to a solution through successive iterations. Finite element modeling allows for models with thousands of individual triangular sections and points to be efficiently solved on a desktop computer. In finite element analysis, finer meshes converge to more precise results. For this simulation, it was found that a model with approximately 10,000–13,000 elements was very precise (after modeling with 100,000 or more elements, the solution varies only slightly, less than 1%). The lower number of elements allowed for a fast solution time and many different tests and variables to be considered.

2.1. Electrical model

All the current generated in the fuel cell must pass through the diffusion layers and graphite to escape the cell. Sometimes an afterthought in the design of the fuel cell, voltage drops due to resistive losses can significantly affect the operating characteristics of the cell. Fortunately, modeling the DC currents in the fuel cell is straightforward with the present model. Use is made of the electrical conduction equation, shown in Eq. (3), which has previously been used to model the currents in fuel cells [7].

$$\nabla(-\sigma\nabla\phi) = 0 \tag{3}$$

The boundary layer at the diffusion layer to membrane interface is also an important consideration. Normally, voltages must be equal at the boundaries between the sections, but in the case of the fuel cell, current is generated at the interface. The current source occurs here because the catalyst layer is treated as if it is

Note: The * indicates a symbol, superscript, or subscript that occurs multiple times, either as different species or on different terms.

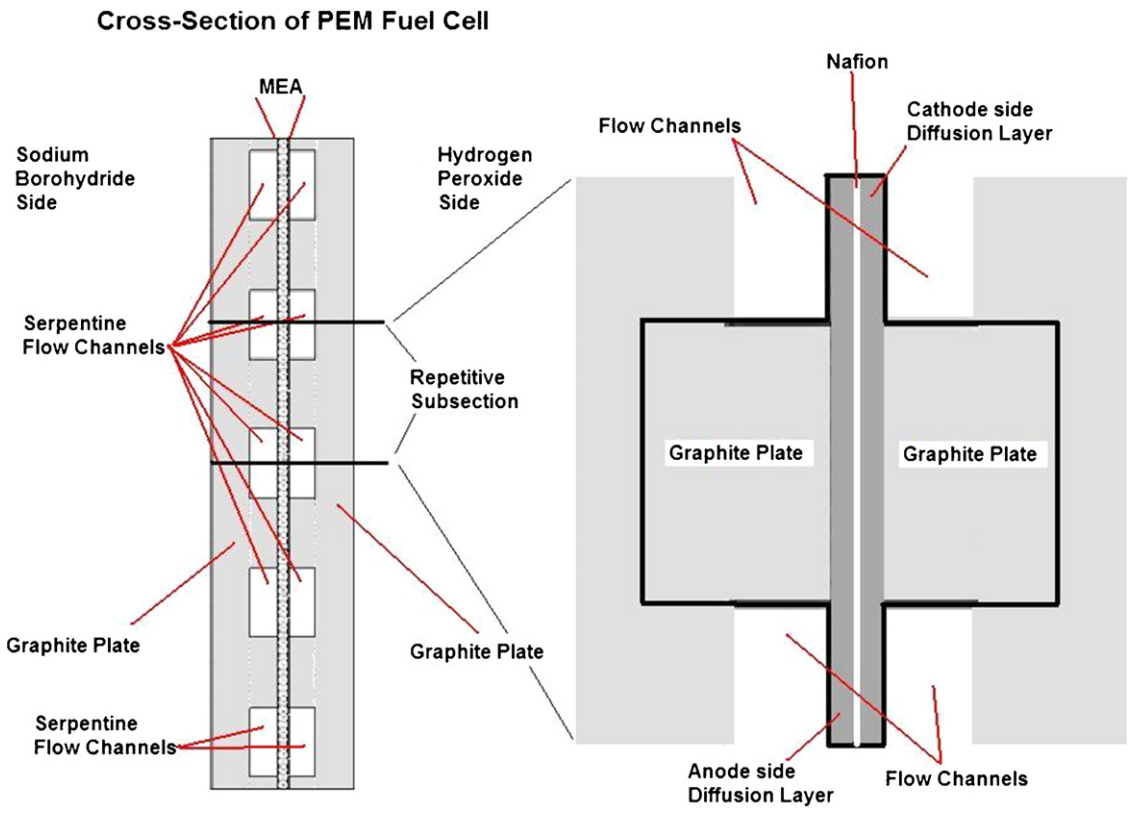

Fig. 1. MEA cross section.

located on the surface of the Nafion membrane. This is another simplification since the catalyst in the actual cell is distributed over the diffusion layer. While some error is introduced, following normalization of the exchange current [4], any error caused is thought to be minimal. The Butler–Volmer equation is then used to model the current generated at the membrane interface [8].

$$i = i_0 \left[\exp\left(\frac{-n\beta F\eta}{RT}\right) - \exp\left(\frac{-n[1-\beta]F\eta}{RT}\right)\right] \tag{4}$$

Eq. (4), the generic Butler–Volmer equation, is separated into anode and cathode terms (the two sides of the membrane) and includes the normalized reactant concentrations. In addition, the overpotential of the anode and cathode must be considered. Here the overpotential is simply labeled η, but it must also be separated into anodic and cathodic terms in Eqs. (5) and (6) [5].

$$i_a = i_{0,a}\frac{w\mathrm{NaBH_4}}{w\mathrm{NaBH_{40}}}(\exp(\alpha_a f\eta_a) - \exp(-\alpha_a f\eta_a))$$
$$\eta_a = \phi_{d1} - \phi_m - \phi_a^{eq} \tag{5}$$

$$i_c = i_{0,c}\frac{w\mathrm{H_2O_2}}{w\mathrm{H_2O_{20}}}(\exp(\alpha_c f\eta_c) - \exp(-\alpha_c f\eta_c))$$
$$\eta_c = \phi_{d2} - \phi_m - \phi_c^{eq} \tag{6}$$

The Butler–Volmer equation can be easily modified to a more useful, alternative version that appears to be more robust when solving the equation numerically while also being mathematically identical. In this version, the hyperbolic identity of Eq. (7) is used to eliminate the exponentials, forming Eq. (8).

$$\cosh(x) = \frac{1}{2}(\exp(x) - \exp(-x)) \tag{7}$$

$$i_a = 2i_{0,a}\frac{w\mathrm{NaBH_4}}{w\mathrm{NaBH_{40}}}\cosh(\alpha_a f\eta_a)$$
$$i_c = 2i_{0,c}\frac{w\mathrm{H_2O_2}}{w\mathrm{H_2O_{20}}}\cosh(\alpha_c f\eta_c) \tag{8}$$

Since the current generation is reliant upon reactants being delivered to the membrane, convection and diffusion in the diffusion layer are crucial portions of the model. At the same time reactant depletion and product generation occurring at the membrane interface depends on the current.

The electrical boundary conditions are very simple; the two graphite ends of the cell are considered to be at constant voltage. One side is the fuel cell voltage, the other is 0 V. In the equations, it is only the difference in the two ends that affects the results so this could represent any cell in a fuel cell stack. Internal boundary conditions simply follow Kirchhoff's Circuit Laws. The top and bottom boundary conditions are electrically floating since the repetitive array can be mirrored along these lines, meaning current does not flow [6].

2.2. Fluid model

There are many different ways to address momentum balance in a fluid velocity field, but the diffusion layer in a fuel cell

is relatively unique due to its porous nature. For this reason it is convenient to use Darcy's empirical law for laminar flow in packed beds, indicated in Eq. (9). In Darcy's law, the fluid velocity is proportional to the change in pressure and inversely proportional to the viscosity [9].

$$v' = -\frac{k\Delta p}{\mu} \tag{9}$$

The velocity profile and pressure differential are solved for in the model, but the permeability and viscosity are dependent on the fluids and the diffusion layer used.

The mass balance in the fuel cell incorporates the fluid velocity from the momentum balance with the movement of the reactants and products. Modeling mass balance in a two-phase, hydrogen/oxygen (H_2/O_2) fuel cell is quite complicated. The reactants arrive as gasses but also must diffuse through a water layer at the membrane. However, for the all-liquid (i.e., *single*-phase) $NaBH_4/H_2O_2$ fuel cell, mass balance is greatly simplified. The single-phase system is modeled in a straight forward manner using standard convection and diffusion equations. These are even simpler if temperature gradients are considered to be minimal, which is a reasonable assumption in the present case given steady-state operation of the fuel cell and the high thermal conductivity of the liquid reactants. The standard diffusion equation is Fick's Law in Eq. (10).

$$\nabla \cdot (-D_i \nabla i) = R - \boldsymbol{u} \cdot \nabla i \tag{10}$$

The subscript and symbol i refers to the species, or reactant and product in the region. For example, the anode has sodium borohydride, sodium metaborate, and water for species.

Eq. (10) must to be considered for each reactant and product species used and needs to be constrained to the corresponding diffusion layer. For the current model, the reactions do not occur in the diffusion layer itself, but instead only at the membrane interface. Hence, $R = 0$ in the diffusion layers. The fluid velocity $\boldsymbol{u}$ is determined using Darcy's law, requiring the coupling of these differential equations.

The mass balance boundary layers are dependent on the sources and the sinks in the system. For reactants, the sources occur at the inlets and outlets of the flow channels, which are considered to be at constant concentration. The sinks for the reactants occur at the membrane interface and are dependent on the current. The sources for the products occur at the membrane interface and are also dependent on the system current. The flow channels are assumed to have no products and thus serve as sinks. The boundary layer equations for the reactants have the form shown in Eq. (11).

$$-\mathbf{n} \cdot N = N_0 \qquad N = -D_i \nabla i + i\boldsymbol{u} \tag{11}$$

In summary, the currents are determined using the Butler-Volmer equations, the fluid velocity with Darcy's Law, the voltages with the DC media equations, and the reactant concentrations with convection and diffusion.

Table 1
Fuel cell parameters

Parameter	Value	Parameter	Value
σ_{Nafion}	15 S m^{-1}	p_{in}	1.013e−5 Pa
$\sigma_{Diffusion}$	2500 S m^{-1}	p_{diff}	500 Pa
$\sigma_{Graphite}$	16670 S m^{-1}	$D_{H_2O_2}$	3.47e−9 m^2 s^{-1}
κ	1.22e−11 m^2	D_{NaBH_4}	3e−9 m^2 s^{-1}
μ_a	1.5 cP	D_{NaBO_2}	1.23e−9 m^2 s^{-1}
μ_c	1 cP	Drag	3

3. Calculations of parameters

Many of the parameters necessary to simulate the fuel cell have been acquired through experimental means or published values, including the conductivities, permeabilities, diffusion coefficients, and viscosities. These parameters are included in Table 1.

It is commonly accepted in literature that three water molecules are dragged across the membrane with each hydrogen ion [8]. We assume that Nafion drag coefficient will remain unchanged in the present all-liquid case.

It is also necessary to determine the parameters used in the Butler–Volmer equations. A Hydrogen half-cell was constructed and used to determine the exchange current density and additional parameters such as the Tafel slope. The reversible potential of each cell half was determined using the Gibb's Free Energies applied to the reactants and products in each reaction.

4. Simulation and results

Fig. 2 is the *I–V* curve for the model created. The figure shows the effects of the anode and cathode activation overpotentials and the ohmic losses. The cell achieves a power density of about 0.31 W cm^{-2} for this region of the membrane. Some advanced $NaBH_4/H_2O_2$ experimental cells have achieved power densities of 1.5 W cm^{-2}, but the normal version this model treats typically generate <0.5 W cm^{-2} [1–3].

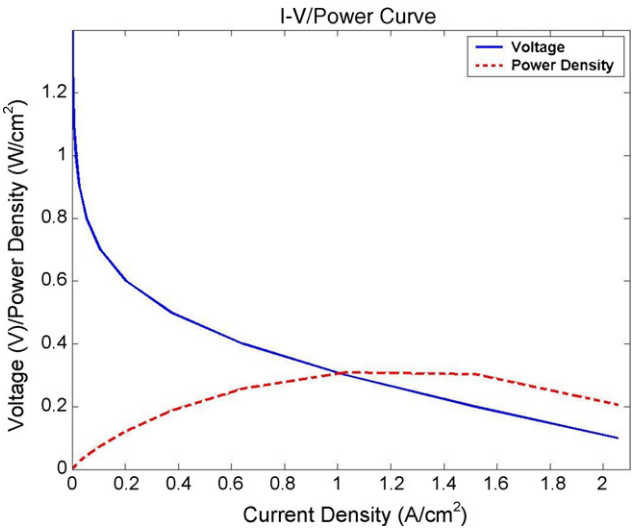

Fig. 2. *I–V* curve of reference model.

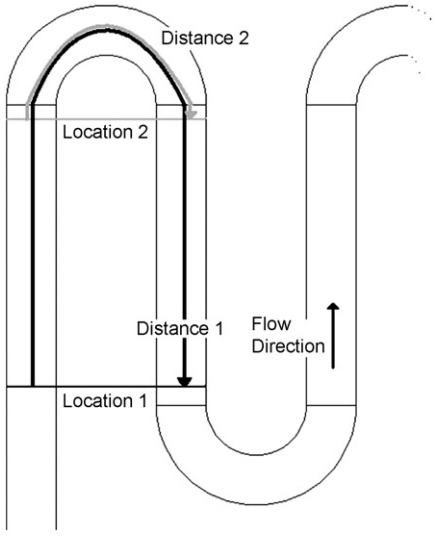

Fig. 3. Varying channel distances in serpentine design.

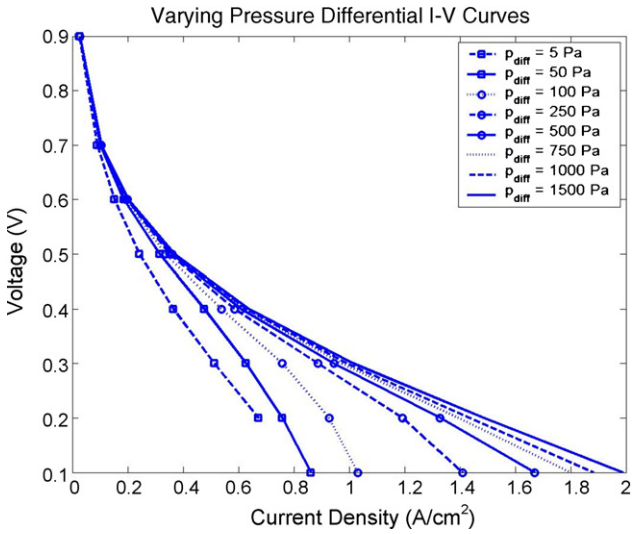

Fig. 4. Varying pressure differential.

Based on Fig. 2, the model represents the all-liquid fuel cell fairly well. However, simply generating a model is not the only goal. Dimensions and parameters within the model are to be varied to better understand how they affect the overall performance of the cell. First, the pressure differential between the two channels is varied. Then, the current collector land area to channel width ratio is varied versus the permeability and conductivity of the diffusion layer. The comparisons are done using the *I–V* curves or power density comparisons, but additional information using other plots is provided when useful.

The pressure differential between the channels is controlled by two separate and independent factors: the channel velocity and the location in the cell. An increased channel velocity creates a higher-pressure drop across the entire length of the flow channel, resulting in an increased pressure differential between two neighboring channels. The effects of varying channel velocity (and hence a varying pressure differential) are important to understand and characterize. In addition, the pressure differential is dependent on the location within the cell. The varying channel distance in serpentine designs, illustrated schematically in Fig. 3, occurs because of the serpentine design of the flow channel. When the channel reverses directions on itself, there will be less pressure differential between the two channels; the fluid has traveled less distance so there will be a smaller pressure drop between the two points in the channel.

The model results shown in Fig. 4 indicate that an increased pressure differential across the inlet channels raises the *I–V* curve, resulting in higher power. The important characteristic of the plot occurs for the pressure differential is at and below 500 Pa; the *I–V* curve starts sloping downwards at higher currents. The reduced currents are from mass transport effects; the reactants are unable to permeate through the diffusion layer to the membrane surface for reaction. Intuitively, this makes sense; the higher-pressure differential creates a higher fluid velocity between the channels, allowing more reactants to permeate the diffusion layer and reach the membrane.

With the higher pressures, the fluid velocity is dramatically increased between the two channels and reactant maintains higher concentrations under the current collector. The reactants maintain the initial concentration much further under the current collector for the higher velocities. For the remainder of the simulations, the pressure differential across the channels remains constant at 500 Pa.

Next, the current collector land area is varied. Basically, varying the land area is akin to varying the channel width, so instead of simply varying the land area, the land area to channel width ratio is varied. The total width of land area plus channel is kept constant at 4.4 mm. By varying the ratio while also using multiple values for the conductivity and the permeability of the diffusion layer, it is possible to develop trends associated with the land area. Fig. 5 shows the maximum power density achieved by the cell versus the land area to channel width ratio; as indicated, the diffusion layer permeability value is also varied, in this plot.

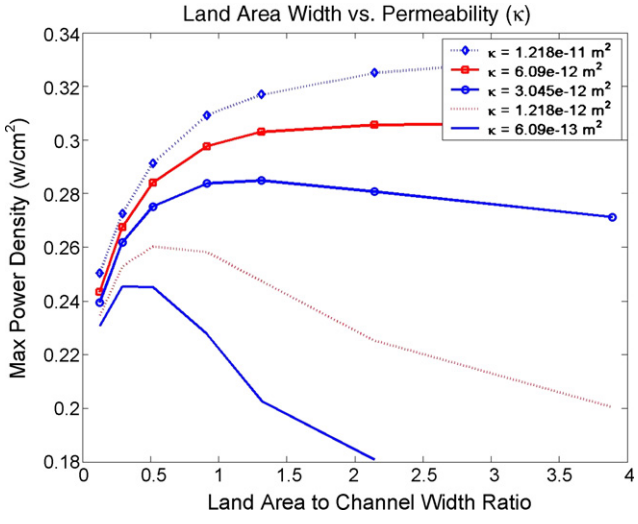

Fig. 5. Land area width vs. permeability values.

There are several competing effects illustrated in Fig. 5. First, for the mid-to-low permeability values (Kappa $< 3.045 \times 10^{-12}$ m^2), high ratios greatly reduce the power capabilities as a result of mass transport effects. As discussed previously, the fluid velocity under the land area is highly dependent on the permeability. With this in mind, a large land area would logically create problems with fluid velocity, resulting in a lack of reactants under the membrane.

The other effect seen in Fig. 5 is the limited conductivity of the diffusion layer. All the current that passes through the graphite current collector must also spread out to cover the membrane surface to react evenly across the entire surface; for narrow current collectors (low ratios), the diffusion layer provides enough resistance to inhibit this "spreading out" of the current to cover the membrane surface. Fig. 6 illustrates the maximum power density achieved while varying the land area to channel width ratio for several different conductivity values.

As the conductivity increases, a one-to-one ratio of the current collector land area to flow channel width becomes optimum. For lower conductivities, having a wider land area and narrower channel is shown to be more effective. One noticeable trend is the reduced power density for all conductivities when the ratio is less than one, which illustrates how difficult the "spreading out" of the current is, even at high diffusion layer conductivities. All the computations above were conducted with a diffusion layer thickness of 0.2 mm.

Different diffusion layer thicknesses would probably result in different peaks, but the trends would still be the same. The reason for the reduction at high land area to channel width ratios most likely results from mass transport effects; the cause and effects of mass transport have already been discussed while varying the pressure differential and the permeability values.

As the conductivity increases, the current achieved at the center of the flow channel increases, which intuitively makes sense; the higher conductivity allows the current to "spread out" more, achieving the higher current density in that region. The narrower land area lowers the current density in the center of the flow channel for both conductivities. The narrowest land area tested actually reduced the current density in the center of the flow channel from 13 to 43%, depending on the conductivity. This indicates the difficulty that the current has in reaching the membrane under the flow channel due to the increased resistance encountered.

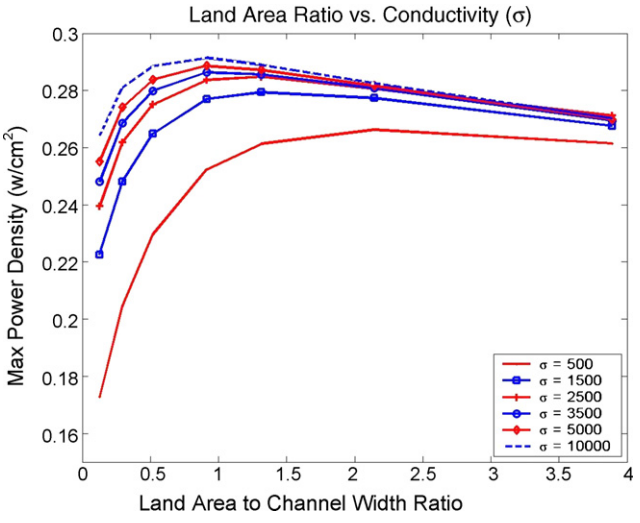

Fig. 6. Land area width vs. conductivity.

5. Discussion

There are several conclusions to be made based on the trends observed while varying the pressure differential across the two flow channels. First, operating at a higher flow velocity will create higher-pressure differentials throughout the fuel cell, increasing the reactant flow to the membrane and increasing the average power through the cell. However, high velocities and the resulting pressure differential from inlet to outlet of the reactants may not be practical. Second, the power density in the cell is strongly dependent on location in the cell. As discussed previously, there is a varying pressure differential across the two channels depending on the location along the serpentine channel; this varying pressure differential creates a varying power density that is low when the serpentine wraps around on itself and high when turning away. Achieving a reduction in power density variations by redesigning the flow channel layout is not a trivial task, and has not been attempted though it merits further study.

Finally, varying the current collector land area to channel width ratio resulted in observations as well. The optimum ratio is highly dependent on the permeability and conductivity of the diffusion layer. The trends were determined for the two parameters independently, but in general, lower ratios reduce the maximum power reached regardless of the permeability or conductivity. For low permeability values, the maximum power density was also reduced for large ratios due to mass transport effects. For conductive membranes, the optimum land area to channel width ratio is approximately one-to-one, meaning equal widths for both. For lower conductivity membranes, the optimum ratio increases slightly. The ratio with the highest power depends on the permeability and conductivity of the diffusion layer, leading to the conclusion that an optimum solution can be determined through simulation if a specific conductivity and permeability are provided.

6. Conclusion

A cross-sectional, all-liquid fuel cell model was created and simulated using finite element modeling software. The pressure differential between the flow channels and the land area to channel width ratio were altered to determine the effects on the power density in the model. Furthermore, permeability and conductivity values were varied, with a trend indicating an optimum geometry exists to maximize the power density for a given MEA permeability and conductivity. Based on research from the studies performed, an optimum land area to channel width ratio can be determined for a specific fuel cell (assuming known permeability, conductivity, and thickness of the diffusion layer). In further studies, given geometry of the fuel cell, the optimum

characteristics of the diffusion layer can be determined through simulation, which would aid the choice of materials.

Acknowledgements

The authors thank NPL Associates, Inc. and fellow researchers (N. Luo, J. Mather, G. Hawkins, and L. Guo) for tremendous support while performing the simulation study. The work reported here was supported by DARPA SB04-032. Continuing studies are supported by DARPA/AFRL.

References

[1] N. Luo, G.H. Miley, P. Shrestha, R. Gimlin, R. Burton, J. Rusek, F. Holcomb, Presented at Third International Energy Conversion Engineering Conference, San Francisco, California, August, 2005.

[2] N. Luo, G.H. Miley, P.J. Shrestha, R. Gimlin, R. Burton, G. Hawkins, J. Mather, J. Rusek, F. Holcomb, Presented at Eighth International Hydrogen Peroxide Propulsion Conference, Purdue University, West Lafayette, Indiana, September, 2005.

[3] N. Luo, G.H. Miley, J. Mather, R. Burton, G. Hawkins, R. Gimlin, J. Rusek, T.I. Valdez, S.R. Narayanan, AIP Conf. Proceedings, STAIF 2006, 2006, pp. 209–221.

[4] E.D. Byrd, Modeling a sodium borohydride and hydrogen peroxide fuel cell using COMSOL Multiphysics, M.S. Thesis, UIUC, May 2006.

[5] T. Berning, D.M. Lu, N. Djilali, J. Power Sources 106 (2002) 284–294.

[6] COMSOL Multiphysics chemical engineering module technical staff, The Proton Exchange Membrane Fuel Cell, COMSOL Multiphysics, 2005.

[7] B. Carnes, N. Djilali, J. Power Sources 144 (2005) 83–93.

[8] G. Hoogers (Ed.), Fuel Cell Technology Handbook, CRC Press, Boca Raton, 2003.

[9] C.J. Geankoplis, Transport Processes and Separation Process Principles, fourth ed., Prentice Hall Professional Technical Reference, Upper Saddle River, 2003.